Coherent dynamics of multilevel systems

A. Amirav, U. Even, Joshua Jortner, and L. Kleinman

Coherent dynamics of multilevel systems

A. Amirav, U. Even, and Joshua Jortner

Department of Chemistry, Tel-Aviv University, Tel Aviv, Israel

L. Kleinman

Department of Physics, The University of Texas at Austin, Austin, Texas 78712

In this paper we report the results of an experimental study of the coherent dynamics (CD) of the $(2J + 1)$, with $J = 1$, $2\cdots6$, low-field, equally spaced Zeeman components of the oxygen molecule O_2^{32} (O^{16}–O^{16}) and O_2^{34} (O^{16}–O^{18}) driven by a radio frequency (rf) field in a supersonic molecular beam. A supersonic molecular beam magnetic resonance spectrometer has been employed in the "flop out" mode, where two intense inhomogeneous magnetic fields are antiparallel, so that the resonating Zeeman levels are defocused at the detector, diminishing the beam intensity. The experimental signal interrogates the total number of molecules in a given total angular momentum state J which changed their initial M_J component. The rf amplitude spectroscopy has been applied to study the dependence of the signal on the amplitude of the rf field for various Zeeman manifolds on-resonance, and to investigate the dependence of the signal on the rf frequency. An analytical solution for the coherent dynamics of a spin J system driven by an rf field, which is valid both for on-resonance and for off-resonance situations, was utilized for the analysis of the experimental data. This confrontation between experiment and theory elucidated some of the universal features of the CD of multilevel systems. Inhomogeneous dephasing of the CD effects, which is due to the velocity distribution in the beam, was quantitatively analyzed, providing a novel method for the determination of translational temperatures in supersonic beams.

I. INTRODUCTION

Two-level model systems have been extensively explored for the understanding of radiative interactions and the resulting coherent optical effects in atoms and molecules.[1] These classical studies of the Rabi two-level problem[1] were extended[2] to explore coherent effects in NMR and optical spectroscopy, which involve two-photon transitions in three-level systems and in multilevel systems. There has recently been considerable progress in the understanding of the dynamics of multilevel systems which are near-resonantly coupled to an electromagnetic field.[3-6] The familiar two-level Rabi problem[1] can be generalized within the framework of the rotating wave approximation to handle the time evolution of a multilevel system with the effects of intramolecular reactive relaxation, such as autoionization or predissociation, being incorporated in a self-consistent manner.[3-6] The time dependent transition amplitudes are determined by linear first-order differential equations. The solution of the dynamics of a N level, "isolated," collision-free atomic or molecular system requires the diagonalization of a NXN symmetric matrix. Recently, quite extensive numerical calculations were conducted for near-resonant multiphoton excitation of model systems, such as one-dimensional[3b,5,7] and three-dimensional[8] anharmonic oscillators. An alternative approach involved the derivation of exact analytical solutions for simple multilevel model systems, such as an equally spaced, equally coupled (ESEC) ladder[6] or an equally spaced manifold where coupling between adjacent states is isomorphous with that for a harmonic oscillator,[6] both systems being studied for on-resonance radiative interactions. One of the motivations for exploring such analytical solutions is to establish some universal characteristics of the coherent dynamics (CD) of sparse multilevel systems. Unfortunately, idealized model systems, such as the ESEC

ladder are not encountered in real life. An interesting system which falls into the category of analytically soluble models and whose properties can also be explored experimentally involves N equidistant levels, with the radiative coupling which prevails between adjacent levels being determined by the xth component, J_x, of the angular momentum J. From the point of view of general methodology, analytical solutions can be derived for the CD of such systems, both for resonance as well as for off-resonance interactions. From the experimental point of view, such systems correspond to the dynamics of a manifold of N equally spaced low-field Zeeman components of a spin J in a rf field. In this paper we report the results of an experimental study of the CD of the $N = (2J+1)$ (with $J = 1, 2, \ldots, 6$) low-field Zeeman components of the oxygen molecule [O_2^{32} and O_2^{34}] in a rf field by utilizing the techniques of magnetic resonance spectroscopy in supersonic molecular beams.[9,10] The experimental and theoretical exploration of these equally spaced multilevel systems is of interest because of several reasons:

(1) The extension of the celebrated two-level Rabi problem to a realistic multilevel system is of intrinsic interest, providing a direct experimental test for an analytically soluble nontrivial problem of quantum dynamics.

(2) The response of multilevel systems driven by an electromagnetic field is of considerable current interest in relation to high-order multiphoton photodissociation,[11-13] isomerization,[14] and ionization[15] of collision-free polyatomic molecules. In the lower molecular energy range (range I)[5] the molecular level structure is sparse and the multiphoton excitation process can be described in terms of near-resonant radiative coupling with an N level system, which is coherently driven by the electromagnetic field.

(3) The experimental results provide an alternative spectroscopic method for the assignment of the angular momentum states of paramagnetic molecules.

(4) Studies of the dephasing effects on the coherent dynamic process provide a new method to probe the velocity distribution in supersonic beams, enabling the simultaneous determination of translational and rotational temperatures.

(5) The degree of the change of the populations of the Zeeman levels in a rf field under the conditions of coherent excitation can be extracted from the present experiments. The degree of maximum level reversal in such a multilevel system is important for the assessment of the efficiency of isotope separation in supersonic molecular beams using rf spectroscopy, which was proposed and studied by Amirav and Even.[16]

II. OUTLINE OF THE EXPERIMENT

Molecular beam magnetic resonance spectrometers[17,18] function by selective deflection and focusing of paramagnetic species according to their spin states. The addition of a supersonic nozzle beam source to the spectrometer provides a molecular beam characterized by high intensity, highly uniform velocity distribution, and low rotational temperature.[19-21] The advantages of using supersonic molecular beams for the study of the CD of two-level systems were demonstrated by Klemperer and colleagues.[22] We have utilized a magnetic resonance spectrometer with a supersonic source to study the dynamics of the low-field Zeeman components originating from various J values of $O^{16}-O^{16}$ and of $O^{16}-O^{18}$. The basic arrangement of the supersonic molecular beam magnetic spectrometer is shown in Fig. 1. The supersonic beam of oxygen is transferred through three successive magnetic fields. The first magnet, an inhomogeneous gradient field magnet, exerts a transverse force on the molecules and aligns their angular momentum (spin) states. These spin states correspond to the M_J components of the total molecular angular momentum in the case of rotation–electronic spin coupling or to electronic spin M_S components in the high magnetic field Paschen Back limit. This force causes spatial separation of the beam constituents according to their spin states. The second magnet creates a low homogeneous magnetic field and contains a rf antenna. Tuning this low magnetic field or the rf frequency to resonance between the Zeeman-split M_J states causes spin flipping in the beam. The third magnet, a gradient field magnet, is directed so that its gradient field is antiparallel to the first magnet and it focuses back the molecular beam. Molecules which had their spin state changed by resonance with the rf field will not be refocused by the third magnet and the beam intensity at the detector will be diminished. This mode of operation involves a "flop out" mode, where the two gradient fields are antiparallel, the resonating M_J states are defocused at the detector, thus diminishing the total beam intensity. Figure 1 shows a schematic trajectory of the $J=1$ three level system in the magnetic spectrometer. Our experiment essentially interrogates the total number of molecules in a given J state of O_2, which have changed their
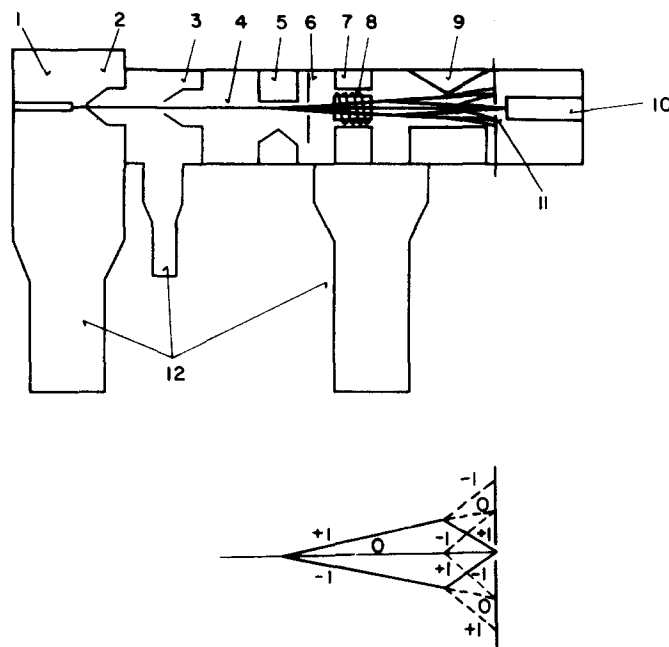

FIG. 1. The basic arrangement of the supersonic molecular beam resonance spectrometer is portrayed in the upper part of this figure. The components of the system are: 1. Nozzle. 2. First skimmer. 3. Second skimmer (collimator). 4. Supersonic molecular beam. 5. A magnet (inhomogeneous field). 6. Beam defining slit. 7. C Magnet (homogeneous field). 8. rf antenna. 9. B Magnet (inhomogeneous field). 10. Molecular beam detector. 11. Detector slit. 12. Vacuum diffusion pumps. The lower part of the figure presents the trajectories for the different M_J levels of the $J=1$ three-level system in the "flop-out" mode. The solid lines correspond to trajectories of these molecules which have not changed their initial M_J state while dashed lines denote the trajectories of those molecules which have changed their initial M_J state. The numbers $+1$, 0, and -1 represent the M_J values.

initial M_J component. The signal was monitored at a fixed frequency corresponding to resonance between adjacent M_J levels vs the amplitude of the rf field or, alternatively, at a fixed rf field amplitude vs the field frequency. These results of rf amplitude spectroscopy provide central information regarding the CD of $N=(2J+1)$ level systems which are practically equidistant. Furthermore, dephasing effects originating from the (small) spread of the velocity distribution in the supersonic beam, which erode the phase coherence, were investigated by our techniques.

III. SOME EXPERIMENTAL DETAILS

The molecular beam magnetic spectrometer with the intense supersonic nozzle (see Fig. 1) was described elsewhere.[16] We shall just consider some features of this apparatus relevant for the present experiment. The rapid expansion of the molecular oxygen or of oxygen–argon mixtures through a 100 μ nozzle into a vacuum creates an intense, low-temperature oxygen supersonic beam. The central core of this beam is skimmed, collimated, and transferred through three successive magnetic fields. Magnet A exerted a field of 9 kG and a field gradient of 23 kG/cm, while magnet B provided a field of 7 kG and a field gradient of 17 kG/

cm. The homogeneous field magnet C gave a field of 3 G. The rf antenna had a flat frequency response up to 300 MHz and was operated in the range 0–5 MHz. After passing through the magnetic spectrometer the beam (signal) was detected by a throttled ionization gauge or by a quadrupole mass spectrometer (Riber GMM 16).

In our experiments two modes of operation were employed: (a) Amplitude dependence of signal. The rf amplitude was changed at a constant frequency. The signal was scanned vs this rf amplitude using an xy recorder. The rf amplitude was modulated by a relay at 11 Hz for phase-sensitive detection. (b) Measurements of line shape. The rf amplitude was kept fixed and the rf frequency was changed. The signal was scanned vs the frequency.

The following aspects of the construction of the apparatus have to be emphasized.

(a) In order to prevent line broadening which results in spurious signal "dephasing," the spatial homogeneity of the magnetic field C was better than $1:10^4$. This was achieved by using a magnetic homogenizer[23] constructed by a sandwich of a μ metal and of brass shims.[16] This homogenizer had to be demagnetized before each experiment by external Helmholtz coils in order to prevent local residual magnetism in the μ metal shims.

(b) To prevent time fluctuations of the C field, the power supply for the two deflecting magnets was current stabilized to better than 10 ppm and the C field magnet consisted of a pair of movable permanent magnets.[16]

(c) To ensure a homogeneous rf field the rf antenna was designed to provide a homogeneous rf field throughout the entire cross section of the beam.

(d) To ensure beam focusing at the detector slit, the deflecting force of the A and B magnets were properly adjusted.

(e) To study an equidistant level system the intensity of the C field was chosen to be sufficiently low (~ 3 G) so that quadratic Zeeman corrections are negligible.

The use of low homogeneous magnetic fields results in some undesirable overlap between different transitions, i.e., the $(J=1, K=1)$ and the $(J=2, K=1)$ transitions of O_2^{32}. This overlap, which is further enhanced by power broadening at high rf amplitudes, inhibits a quantitative study of these three-level and five-level systems. A nice and spectrally clean three-level system is provided by the heteronuclear molecule O_2^{34} (O^{16}–O^{18}), whose $(J=1, K=0)$ state is populated and the transitions between the corresponding Zeeman levels are well separated in energy from all other transitions. Enriched O^{16}–O^{18} samples, used in our experiments, were purchased from the Yeda Company of the Weizmann Institute.

IV. ZEEMAN LEVELS OF MOLECULAR OXYGEN

The Zeeman splitting of the rotational states of the $^3\Sigma_g^-$ ground electronic configuration of the oxygen molecule is well understood[24–27] and will only be summarized. The spin angular momentum S ($S=1$) adds vectorially

to the rotational angular momentum K to yield the total angular momentum $\mathbf{J}=\mathbf{K}+\mathbf{S}$, with the eigenvalues $J(J+1)$, where J may have the values $J=K-1$, K, or $K+1$ and where the eigenvalues of the J_z component will be denoted by M_J. Odd rotational states are populated in the homonuclear O_2^{32} (O^{16}–O^{16}) molecule, while the population of all rotational states is allowed in the heteronuclear O_2^{34} (O^{16}–O^{18}) molecule. As O^{16} and O^{18} have zero nuclear spins, each (J, K) level of O_2^{32} and O_2^{34} splits in an external magnetic field into $(2J+1)$ Zeeman levels $|J, K, M_J\rangle$. The energy levels E_{K,J,M_J} of these states in a static magnetic field $\mathcal{H}_0$ are given by[24–27]

$$E_{K,J,M_J} = W^0_{KJ} + M_J f(K, J) + M_J \delta(K, J) , \qquad (\text{IV.1})$$

where W^0_{KJ} are the zero field energies. The linear Zeeman splittings are

$$f(K, J) = (\mu_0 \mathcal{H}_0 / \hbar) g_J(K, J) \qquad (\text{IV.2a})$$

being expressed in terms of the total g values, $g_J(K, J)$, for each (J, K) manifold of states,[24–26] and where μ_0 is the Bohr magneton. Finally, the quadratic Zeeman splittings are

$$\delta(K, J) = d(K, J)[f(K, J)]^2 , \qquad (\text{IV.2b})$$

where the $d(K, J)$ coefficients for O_2 are available.[24–26] The ratio, $Z(K, J)$, between the quadratic term and the linear term is $Z(K, J) \equiv \delta(K, J)/f(K, J) = d(K, J)f(K, J)$. The largest quadratic Zeeman splitting is exhibited for the (1, 1) state with[24–26] $d(1, 1) = 5.664 \times 10^{-11}$ sec, the corresponding linear term under our low-field experimental conditions is $f(1, 1) = 4.405$ MHz, so that $Z(1, 1) \simeq 2 \times 10^{-4}$. We thus conclude that under our experimental conditions the quadratic level splitting is small, the level structure being essentially determined by the linear Zeeman splitting, whereupon the system corresponds to an equally spaced molecular ladder.

Figure 2 portrays a schematic energy level diagram of molecular oxygen. The $K=1$ state gives rise to the $(J=1, K=1)$ three-level systems and to the $(J=2, K=1)$ five-level systems, while the five-level $(J=2, K=3)$, the seven-level $(J=3, K=3)$ and the nine-level $(J=4, K=3)$ systems have parentage in the $K=3$ rotational state. The $K=1$ and $K=3$ states are populated in O_2^{32}. We have studied the coherent dynamics of multilevel systems $(J=1, K=1)$, $(J=2, K=1)$, $(J=2, K=3)$, $(J=3, K=3)$, $(J=4, K=3)$, and $(J=6, K=5)$ Zeeman manifolds of O_2^{32} (O^{16}–O^{16}) as well as the dynamics of $(J=1, K=0)$ Zeeman components of O_2^{34} (O^{16}–O^{18}). Figures 3 and 4 portray the rf spectra of O^{16}–O^{16} and of O^{16}–O^{18} in low magnetic fields exhibiting the transitions $\Delta J = \Delta K = 0$, $\Delta M_J = \pm 1$. To provide a check for the accuracy of our experimental techniques we present in Table I the normalized Zeeman energy levels $f(K, J)/f(1, 1)$ for O^{16}–O^{16} measured by us, which are in excellent agreement with the $g_J(K, J)$ values originally derived by Hendrie and Kusch.[27]

V. COHERENT OPTICAL EFFECTS IN AN EQUALLY SPACED MULTILEVEL SYSTEM

We shall consider now the problem of the dynamics of $N = (2J+1)$ equally spaced low-field Zeeman levels in a static magnetic field $\mathcal{H}_0$, directed in the z direction,
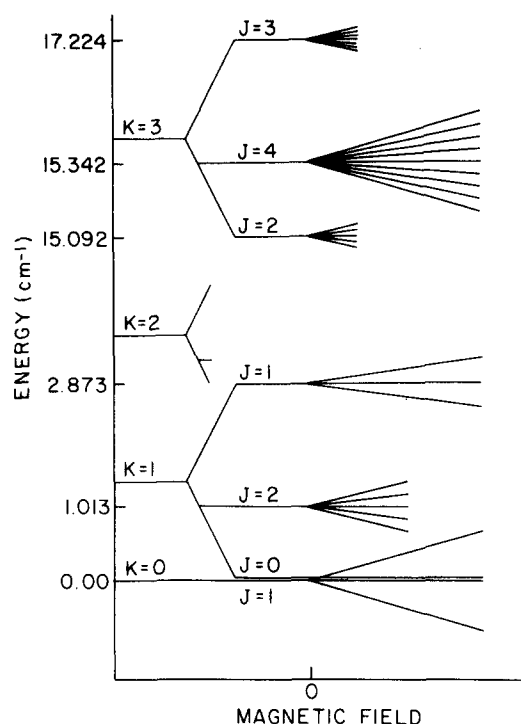
FIG. 2. Schematic energy level diagram of the lowest states of molecular oxygen in a weak magnetic field. The Zeeman splittings are not drawn on scale. The energy levels of $K = 0$, $J = 1$, and $K = 1$, $J = 0$ are very close.

which are driven by an oscillatory rf field, perpendicular to the z axes. We shall refer to this problem, common in magnetic resonance, as the spin J problem. The Hamiltonian for the system is

$$H = H_M + H_{INT}(t) ,\qquad (\text{V.1})$$

where the molecular Hamiltonian can be expressed in the form

$$H_M = \hbar f(K, J) J_z ,\qquad (\text{V.2})$$

while the radiation—matter interaction term is

$$H_{INT}(t) = -2\hbar\beta J_x \cos(\omega t) ,\qquad (\text{V.3})$$

with $\hbar\beta$ specifying the amplitude of the rf field and ω characterizing its frequency. Next, we specify the eigenstates $|J, K, M_J\rangle$ of the molecular Hamiltonian. As we shall be interested only in transitions within the equidistant Zeeman levels within a single (J, K) manifold, we can label these states in terms of J and its z component $M \equiv M_J$, so that we shall denote the relevant molecular states as $|JM\rangle$, with energies E_{JM} and with the level spacing $f(K, J)$ between adjacent M levels.

The dynamics of the system within the framework of the rotating wave approximation (RWA) is outlined in Appendix A. As is apparent from Eq. (A11) of Appendix A, the Hamiltonian matrix is time independent and triagonal with nonvanishing off-diagonal terms only in the two diagonals located above and below the main diagonal. The energetic parameters, which govern the dynamics, are the off-resonance determining $\hbar(\Omega - \omega)$ and the radiative coupling β. The problem of the time evolution of the general spin J system was first solved in 1932 by Majorana[28] by group theoretical methods, while Bloch and Rabi,[29] Schwinger,[30] and Ramsey,[31] have synthesized the transition probabilities for angular momentum J from $2J$ angular momenta of spin $1/2$. An alternative, physically transparent derivation based on the method of unitary transformations was provided by Gottfried.[32] The details of the calculations of the transition amplitudes for this problem utilizing the method of unitary transformations[32] are presented in Appendix B. The probability $P^J_{MM'}(t)$ that the system initially at $|JM\rangle$ will be found in the state $|JM'\rangle$ at time t is given by

$$P^J_{MM'}(t) = \left| d^J_{MM'}(\alpha) \right|^2 ,\qquad (\text{V.4})$$

$$\alpha = 2 \arcsin\left[(\beta/\Delta)\sin(t\Delta/2)\right] ,\qquad (\text{V.5a})$$

$$\Delta = \left[(\Omega - \omega)^2 + \beta^2\right]^{1/2} .\qquad (\text{V.5b})$$

Here $d^J_{MM'}(\alpha)$ is the Wigner rotation function which appears in the $(2J+1)$ dimensional representation of the rotation group. α is the second Euler angle corresponding to rotation of $t\Delta$ about an axis $\hat{n} = \hat{u}_z \cos\phi + \hat{u}_x \sin\phi$, where $\hat{u}_z$ and $\hat{u}_x$ are unit vectors, and $\phi = \arctan[\beta/\Omega - \omega)]$ The parameter α can be given a transparent physical
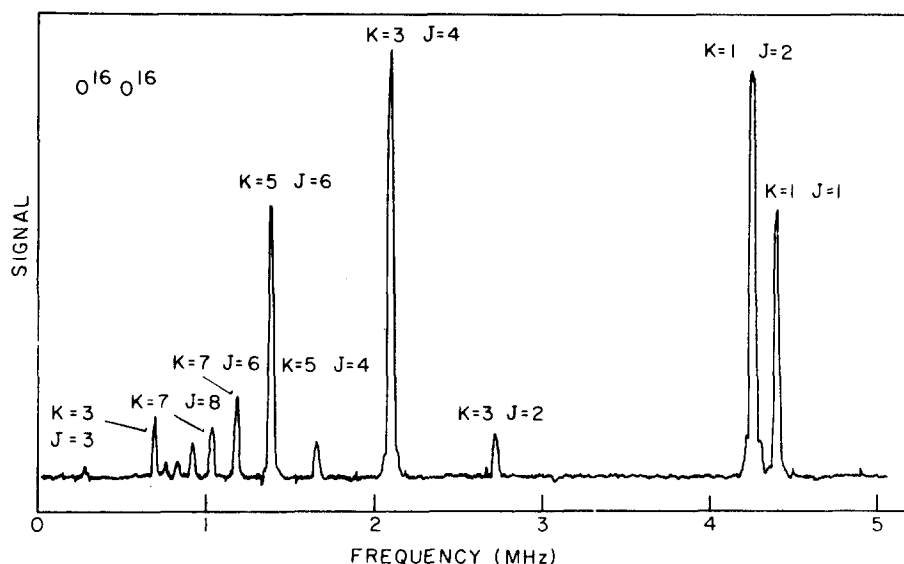

FIG. 3. The experimental Zeeman spectrum of O_2^{32} in a magnetic field of 3.1 G. O_2 at a backing pressure of 50 Torr was expanded through a 100 μ nozzle. The rf amplitude is 0.17 V where the $(J = 1, K = 1)$ line has its maximum. The rotational temperature was 50 K.
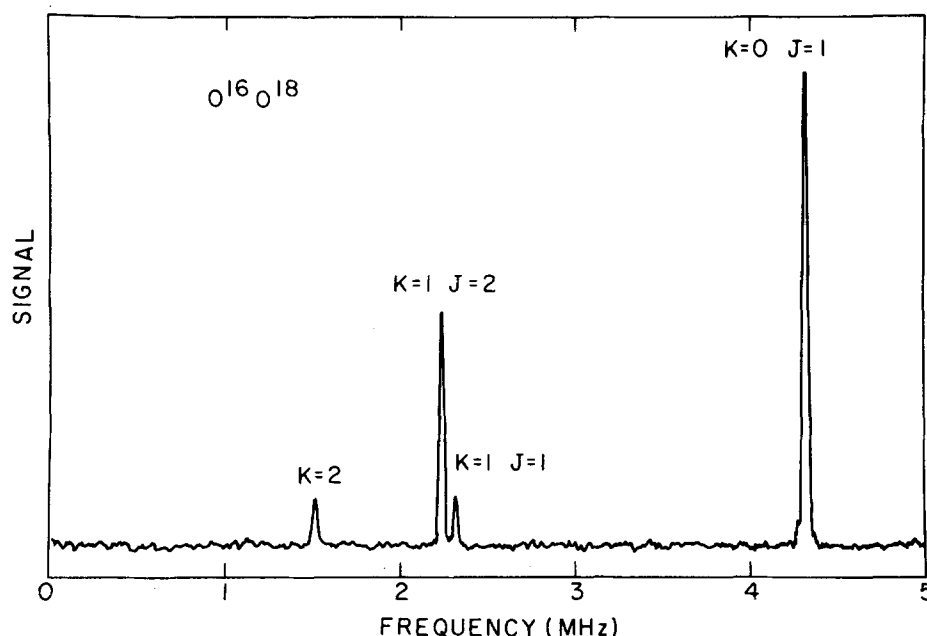
FIG. 4. The experimental Zeeman spectra of $O^{16}O^{18}$ in a magnetic field of 1.8 G. A mixture of 35% He, 60% Ar, and 5% O_2 enriched with O_2^{34} at total pressure of 750 Torr was expanded through a 100 μ nozzle. The rf amplitude was 0.092 V where the ($J=1$, $K=0$) line attains its maximum. The rotational temperature was 2.6 K.

meaning by noting that $\sin^2(\alpha/2)$ represents the transition probability for a spin 1/2 system with the same coupling strength as the general spin J system.[28] Finally, Δ, Eq. (5b), is the generalized Rabi frequency. The explicit form of the Wigner rotation function, which determines the transition probability is[33]

$d_{MM'}^J(\alpha)$

$$= \sum_\mu (-1)^\mu \frac{[(J+M)!\,(J-M)!\,(J+M')!\,(J-M')!]^{1/2}}{(J+M-\mu)!\,(J+M'-\mu)!\,\mu!\,(\mu-M+M')!}$$

$$\otimes[\cos(\alpha/2)]^{2J+M-M'-2\mu}\,[\sin(\alpha/2)]^{2\mu-M+M'} \qquad (V.6)$$

where the summation extends over all values of μ for which the arguments of all the factorials are non-negative. In Appendix C we list the $d_{MM'}^J(\alpha)$ functions for $J=1$, $J=2$, and $J=3$.

Equation (V.4) provides an explicit solution for the problem of the dynamics of an equally spaced ladder of molecular levels, where radiative coupling, given by Eq. (V.3), prevails only between adjacent levels. The analytical solution is applicable, within the framework of the RWA, both for the resonance situation when $\alpha = \beta t$, as well as for the off-resonance case. The problem of a spin J belongs to a class of analytically soluble models for CD of multilevel systems, such as the equal-Rabi and the harmonic-Rabi N level systems, whose characteristics for on-resonance radiative coupling were explored recently by Eberly and colleagues.[6] The solution for the spin J problem is more general as it is applicable for both resonance and off-resonance radiative coupling.

A quite interesting nontrivial special case, which is of some pedagogical interest, involves the simplest generalization of the familiar two-level system, i.e., the $N=3$ case. For the $J=1$ system, $(J_x)_{-10} = (J_x)_{01} = 1/\sqrt{2}$, so that we have an equally spaced equally coupled (ESEC) three-level system where dynamics is governed by Eq. (V.4). A solution to the general problem of an

ESEC N-level system on-resonance, can be provided in terms of classical orthogonal polynomials,[6] the results being equivalent to the classical solution for a chain of identical harmonic oscillators interacting via nearest-neighbor harmonic forces[34] and to the simple quantum mechanical Huckel model for conjugated linear π electron systems.[35] An outline of the treatment of such ESEC systems is given in Appendix D. For the special case of the $N=3$ system on-resonance, the results of the ESEC treatment for $N=3$ are identical with those obtained from Eq. (V.4) for $J=1$. However, for the $J=1$ case, Eq. (V.4) provides us now with a more general solution for the dynamics of an $N=3$ ESEC system in the off-resonance situation.

VI. MODEL CALCULATIONS

As the characteristics of the spin J system coherently driven by an electromagnetic field are interesting and relevant for the interpretation of our experimental data on coherent effects in the low-field Zeeman manifold, we have performed a series of model calculations on this

TABLE I. Frequencies for the low-field Zeeman spectrum of molecular oxygen normalized to $f(1,1)$.

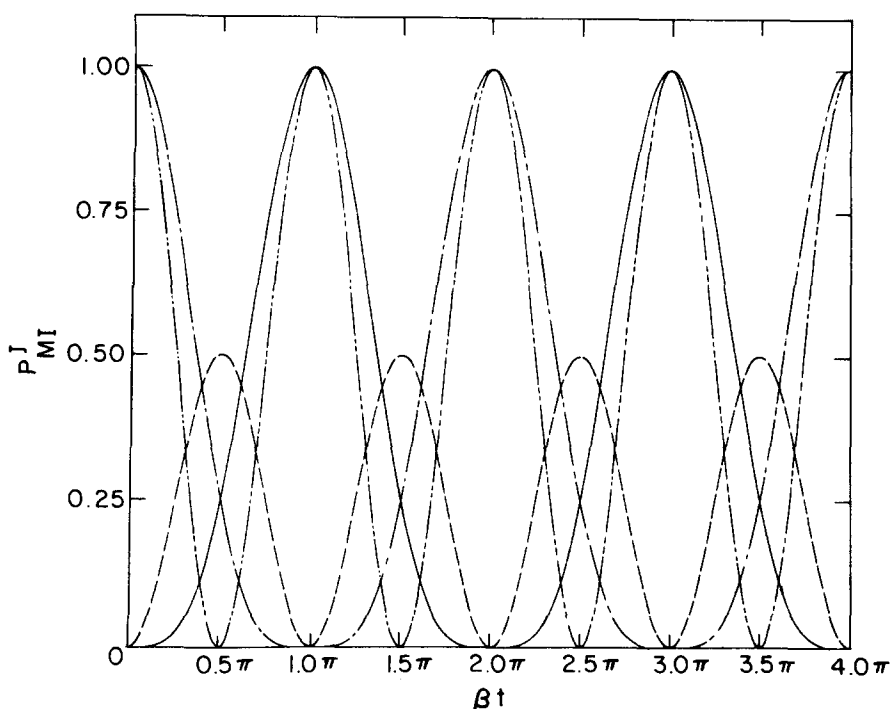| Molecule	K,J	$f(K,J)/f(1,1)$ experimental, present work	$f(K,J)/f(1,1)$ experimental Hendrie and Kusch Ref. 27	$f(K,J)/f(1,1)$ calculated from $g(K,J)$ factors, Ref. 27
O_2^{32}	1,1	1.0000	1.00000	1.00000
	1,2	0.9703	0.96933	0.96931
	3,2	0.6356	0.63573	0.63577
	3,3	0.1666		
	3,4	0.4952	0.49551	0.49550
	5,4	0.3949	0.39526	0.39526
	5,5	0.0670		
	5,6	0.3321	0.33214	0.33217
	7,6	0.2842	0.28437	0.28432
	7,6	0.2491	0.24971	0.24970
O_2^{34}	0,1	1.8179		

FIG. 5. Model calculations for the occupation probabilities $P^1_{MI}(t)$ for a three-level system with $J=1$. $(- \cdot -)$ $M = -1$, $I = -1$, and $M = 1$, $I = 1$. $(- \cdot \cdot -)$ $M = 0$, $I = 0$. $(\underline{\hspace{1cm}})$ $M = -1$, $I = +1$, and $M = +1$, $I = -1$. $(---)$ $M = -1$, $I = 0$; $M = 0$, $I = -1$; $M = 1$, $I = 0$, and $M = 0$; $I = 1$.

system. In Fig. 5 we present the time dependence of the population probabilities, Eq. (V.4), for a three-level system on-resonance. The time dependence of the populations is perfectly periodic. This conclusion is general for an N-level spin J system as, according to Eq. (V.6), the characteristic period of any such system for integer values of J is determined by the condition $\alpha = 2\pi$, so that for the on-resonance situation the system recurs after a time $t = 2\pi/\beta$. The perfect periodicity exhibited by the $J = 1$ system is well known for the equivalent ESEC $N = 3$ system.[6] The behavior of the spin J systems with $J > 1$ is qualitatively different from the characteristics of the corresponding ESEC systems with $N > 3$. For ESEC multilevel systems with $N > 3$ periodicities are absent in the time evolution of the population probabilities. It was suggested by Eberly et al.[6] that the unexpected lack of periodic time evolution for some multilevel model systems, such as the ESEC with $N > 3$, may be a general phenomenon. Our spin J system provides a counterexample in that respect.

We have now to utilize the results of the model calculations to provide a scheme for the analysis of experimental data and consider explicit expressions for the experimental observables which were obtained by the application of rf amplitude spectroscopy to probe the CD of a low-field Zeeman manifold. Our experiment measures the total number of molecules which have changed their M value in the low field rf region, provided that this change of M is amenable to experimental detection in the high-field Stern–Gerlach interrogation region. The probability F^J_M for a molecule in the initial state $|JM\rangle$ to change its M value and that this change be interrogated is

$$F^J_M(t) = \sum_{\substack{M'=-J \\ M' \ne M}}^{J}{}' P^J_{MM'}(t)\,\eta_{(MM')}\,, \qquad (VI.1)$$

where t is the time of flight through the rf region, the

probability $P^J_{MM'}(t)$ is given by Eq. (V.4), and $\eta_{(MM')}$ is the interrogation efficiency function which depends on the high-field Zeeman splitting in the interrogation region. The strength of the inhomogeneous magnetic field (~ 7 kG) in the interrogation range is not sufficient to attain complete decoupling of the electronic spin, as is evident from a cursory examination of the data of Tinkham and Strandberg.[26] In the simplest case, when rotational and electronic spin angular momenta are not decoupled in the interrogation region, $\eta_{(MM')} = 1$ for all M and M'. This is the situation for the $(J=1, K=1)$, $(J=2, K=1)$ manifolds of O_2^{32} and $(J=1, K=0)$ manifold of O_2^{34}. In some other cases there is "bunching" of the states at high magnetic field, so some $\eta_{(MM')}$ have to be taken as zero. Estimates of $\eta_{(MM')}$ can be inferred from the available correlation diagrams.[26]

The signal monitoring the total number of molecules, which have changed their M state, is obtained by thermally averaging the probability (VI.1) over the initial populations of the M levels. The thermal Boltzmann populations Q^J_M for each M low-field Zeeman level for a fixed (J, K) are equal being given by

$$Q^J_M = (2J+1)^{-1}\,. \qquad (VI.2)$$

The signal $\overline{S}^J(t)$ in an ideal beam with a single velocity is proportional to

$$\overline{S}^J(t) = \sum_{M=-J}^{J} Q^J_M F^J_M(t)\,, \qquad (VI.3)$$

where again t is the time of flight through the rf field region. Utilizing Eqs. (VI.2) and (VI.3) the signal [apart from an irrelevant proportionality factor of $(2J+1)$] is

$$\overline{S}^J(t) = \sum_{M=-J}^{J} \sum_{\substack{M'=-J \\ M' \ne M}}^{J}{}' P^J_{MM'}(t)\,\eta_{(MM')}\,. \qquad (VI.4)$$

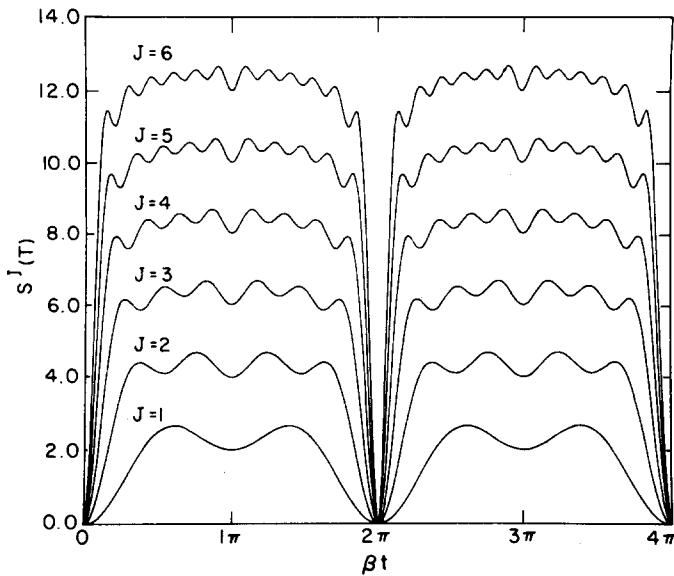For the simplest and most interesting situation when

FIG. 6. Model calculations for the signal function $S^J(t)$, on resonance, Eq. (VI.5), for $J = 1, 2, \ldots, 6$.

the forces exerted on the high-field Zeeman levels in the interrogated region are different for each level, we set $\eta_{(MM')} = 1$ for all values of M and M'. Utilizing the conservation rule $\sum'_{M} P^J_{MM'}(t) = 1 - P^J_{MM}(t)$, the signal, which in this case will be denoted by $S^J(t)$, is given by

$$S^J(t) = (2J+1) - \sum_{M=-J}^{J} P^J_{MM}(t) \qquad \text{(VI.5)}$$

and using Eq. (V.4), we finally get in this case

$$S^J(t) = (2J+1) - \sum_{M=-J}^{J} \left| d^J_{MM}(t) \right|^2 . \qquad \text{(VI.5a)}$$

In general, the signal function depends on the detuning $(\omega - \Omega)$, the amplitude β of the rf field and the time of flight t. It is important to note that this result is applicable both for the on-resonance and for the off-resonance interaction with the rf field.

We have explored the characteristics of the signal function $S^J(t)$, Eq. (VI.5), for the on-resonance situation. For low values of J simple analytical expressions can readily be obtained for on-resonance, i.e., putting $\Delta = \beta$ in Eq. (V.6). For $J = 1$ on-resonance

$$S^1(t) = \left(\tfrac{7}{4}\right) - \cos(\beta t) - \left(\tfrac{3}{4}\right)\cos(2\beta t) \qquad \text{(VI.6)}$$

while for $J = 2$ on-resonance

$$S^2(t) = \left(\tfrac{1}{64}\right)\left[231 - 88\cos\beta t - 68\cos(2\beta t) - 40\cos(3\beta t)\right.$$
$$\left. - 35\cos(4\beta t)\right] , \qquad \text{(VI.7)}$$

For higher values of J, $(J = 3\text{--}6)$, with which we shall also be concerned, it is not advisable to provide such explicit expressions for $S^J(t)$ and we used the fully-fledged expression, Eqs. (VI.5) and (V.6), for the calculations of the signal function. In Fig. 6 we present the dependence of the signal function $S^J(t)$ for the on-resonance situation on the amplitude β of the rf field for $J = 1, 2, \ldots, 6$. These results exhibit the following features:

(a) The oscillating pattern of $S^J(t)$ vs β for multilevel

systems with $N = (2J+1) = 3, 5, \ldots, 13$ marks coherent quantum effects determined by phase relationship between the transition amplitudes of individual levels in each manifold.

(b) The maximum value of the signal function $S^J(t)$ for each value of J is always less than $(2J+1)$. The maximum value is 2.666 for $J = 1$, 4.690 for $J = 2$, 6.899 for $J = 3$, 8.700 for $J = 4$, and 12.700 for $J = 6$, so that it seems that the limiting high J value is $(2J+1) - 0.300$. This feature of multilevel systems differs from the characteristics of a two-level system where the maximum value of $S^{1/2}(t)$ is just unity at $t = 2\pi/\beta$. This characteristic of multilevel systems implies that for a given value of J all the diagonal probability functions $P^J_{MM}(t)$ $(M = -J, \ldots, +J)$ do not vanish at the same value of t.

(c) In the time domain $\beta t = 0, \ldots, 2\pi$ there are $2J$ subsidiary peaks and $(2J-1)$ minima, which originate from out-of-phase growth and decrease of the transition amplitudes of the intermediate levels in the equally spaced ladder.

(d) The signal functions $S^J(t)$ vanish at $t = 2\pi/\beta$ for all integer values of J. Thus, all the diagonal probability functions $P^J_{MM}(t)$ $(M = -J, \ldots, +J)$ assume the value of unity at $t = 2\pi/\beta$, which marks the recurrence time for such equally spaced multilevel systems.

(e) On the basis of the analysis of the time evolution of the population probabilities (Fig. 5), we assert that the on-resonance signal function is periodic, as is evident from Fig. 6.

(f) Dephasing processes will erode the oscillatory pattern. Such inhomogeneous broadening can originate from the distribution of the flight times through the rf field, which will be discussed in Sec. VII. The signal in the dephased system will assume a constant value, independent of β. A cursory examination of Eqs. (VI.6) and (VI.7) for $N = 3$ and $N = 5$ multilevel systems indicates that the completely dephased signal is $(7/4)$ for $J = 1$ and $(231/64)$ for $J = 2$. Complete memory loss would imply that the dephased signal could be 2.00 for $J = 1$ and 4.00 for $J = 2$. The dephased signals predicted on the basis of the theory are lower, demonstrating some of the subtle features of inhomogeneous dephasing in a multilevel system.

Next, we have considered the frequency dependence of $S^J(t)$ for a fixed value of J. In Fig. 7 we present the rf frequency dependence for the three-level system $J = 1$ at a fixed value of the flight time t. The calculations were performed for several values of β. These results will be utilized in Sec. VII for the understanding of the line shapes of the rf spectra.

Finally, we have to consider the interrelationships between the level structure of the Zeeman components in the weak rf field, where excitation is performed, and in the strong field region (of magnets A and B of Fig. 1), where alignment at interrogation is carried out. For $K = 3$ and $K = 5$ the spin-rotation coupling is weaker than for $K = 1$ or $K = 0$, whereupon the assumption of effective coupling between rotational angular momentum and electronic spin in the interrogation region (~7 kG

field strength) breaks down and some of the interrogation efficiency factors, which appear in Eq. (VI.4), differ from unity. Model calculations were conducted for the signal function $\bar{S}^J(t)$, Eq. (VI.4), in the on-resonance situation, for $J = 2$, 3 and 4. The rf amplitude spectra calculated for different grouping of the energy levels in the high-field regions are portrayed in Fig. 8 for $J = 2$, in Fig. 9 for $J = 3$ and in Fig. 10 for $J = 4$. Figures 8(a), 9(a), and 10(a) present the predictions for the limit of strong spin–rotation coupling with $\eta_{MM'} = 1$ for all M and M'. Figures 8(b), 9(b), and 10(b) give the signal calculated for the groupings of the energy levels in the high field according to the correlation diagrams of Tinkham and Strandberg[26] taken at the field of 7 kG. In this case $\eta_{MM'} = 0$ if M and M' belong to the same group while $\eta_{MM'} = 1$ when M and M' are in different groups. In using the correlation diagrams we have disregarded the effects of level crossing with other M_J states. Therefore we have conducted some additional model calculations and in Figs. 8(c), 8(d), 9(c), and 10(c) we display the rf amplitude spectra in the case of symmetrical grouping of the energy levels into three
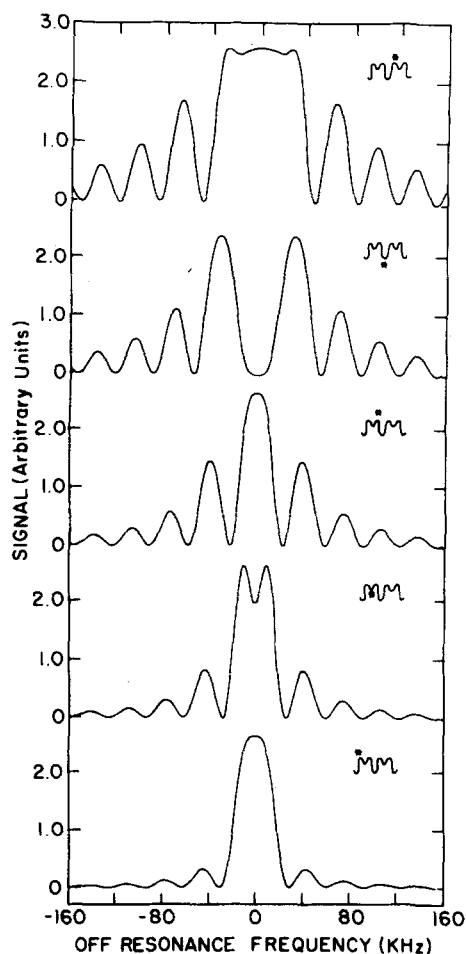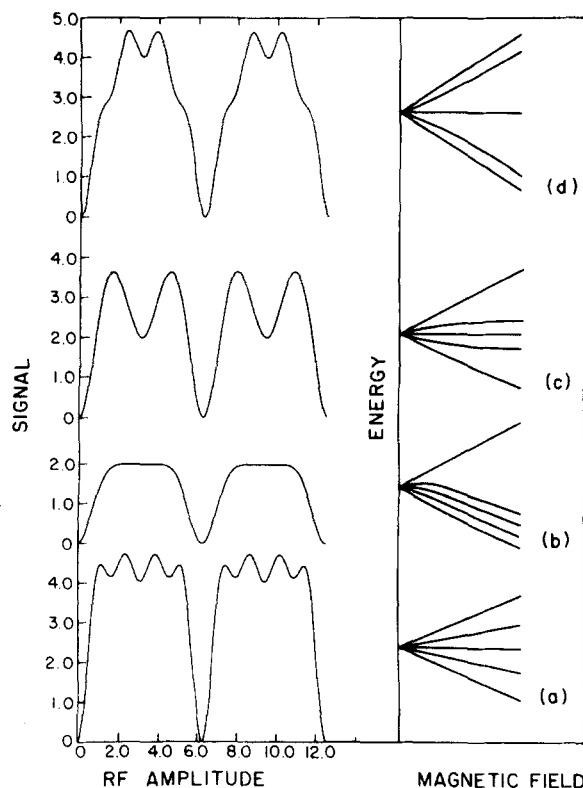

FIG. 8. Model calculations for the general signal function Eq. (IV. 4) on-resonance for a $J = 2$ five-level system. (a) corresponds to $\eta_{MM'} = 1$ for all M and M'. (b) represents the level grouping according to the correlation diagrams of Ref. 26 where $\eta_{MM'} = 0$ for M and M' belonging to the lowest four levels and otherwise $\eta_{MM'} = 1$. (c) and (d) denote symmetric level groupings in bunches of 1, 3, 1 for (c) and 2, 1, 2 for (d).
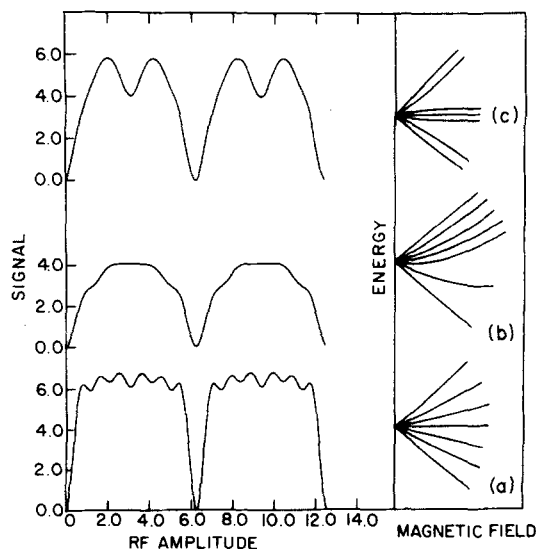

FIG. 7. Model calculations for the frequency dependence of the signal function, Eq. (IV. 5a) for a three-level system $J = 1$. The flight time was kept constant while β was varied so that the values of β correspond to the first three maxima and the first two minima of Fig. 6, as indicated. The values of βt for the five curves displayed, from bottom to top correspond to the values $\beta t = 1.91$, π, 4.37, 2π, and 8.19.

FIG. 9. Model calculations for the general signal function, Eq. (IV. 4), on-resonance for a $J = 3$ seven-level system. (a) corresponds to $\eta_{MM'} = 1$ for all M and M'. (b) represents the level spacing according to the correlation diagrams of Ref. 26, with the levels grouped in bunches of 1, 1, 5. (c) denotes a symmetric level grouping in bunches of 2, 3, 2.
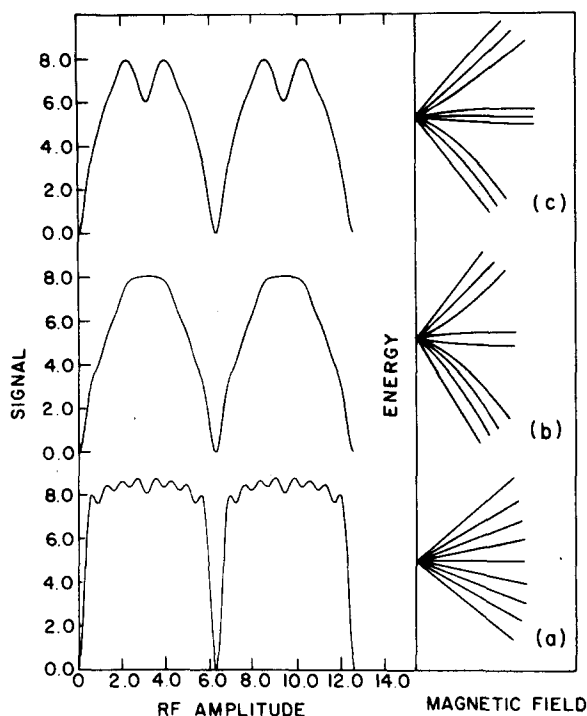
FIG. 10. Model calculations for the general signal function, Eq. (IV. 4), on-resonance for the $J = 4$ nine-level spectra. (a) corresponds to $\eta_{MM'} = 1$ for all M and M'. (b) represents the level grouping in bunches of $4, 2, 3$ according to the correlation diagram of Ref. 26, while (c) denotes a symmetric level grouping in bunches of $3, 3, 3$.

$$F(v) = (v/v_s)^3 \exp\{-(\gamma M^2/2)[(v/v_s) - 1]^2\}, \qquad \text{(VII. 1)}$$

where v is the velocity, v_s the mean velocity, $\gamma = C_p / C_v$ of the gas, and M the Mach number. The time of flight is

$$t = L/v, \qquad \text{(VII. 2)}$$

where L is the linear dimension of the rf antenna, so that the mean time of flight is $t_s = L/v_s$. The signal, $S_A^J(t_s)$ from a beam characterized by the velocity distribution (VII. 1) and the mean time of flight t_s is now obtained by averaging $S^J(t)$ over $F(v)$,

$$S_A^J(t_s) = \int_0^\infty dv\, F(v) S_J(L/v) \left[\int_0^\infty dv\, F(v)\right]^{-1}. \qquad \text{(VII. 3)}$$

An equivalent expression can be written for the signal originating from $\bar{S}^J(t)$. The calculations were conducted by standard numerical integration methods. From the analysis of the rf amplitude dependence of the experimental signal the Mach number and the translational temperature of the supersonic beam were evaluated.

A. Three-level system

We have studied experimentally the three-level system which corresponds to the $(J = 1,\ K = 0)$ manifold of O_2^{34} (O^{16}–O^{18}). At low magnetic fields (see Fig. 3) this manifold, unlike the $(J = 1,\ K = 1)$ manifold of O_2^{32}, is well isolated from any other (J, K) states. Figure 11 shows the experimental dependence of the signal recorded by the mass spectrometer detector in the "flop out" mode of operation of our supersonic molecular beam magnetic spectrometer (see Sec. II). The experi-
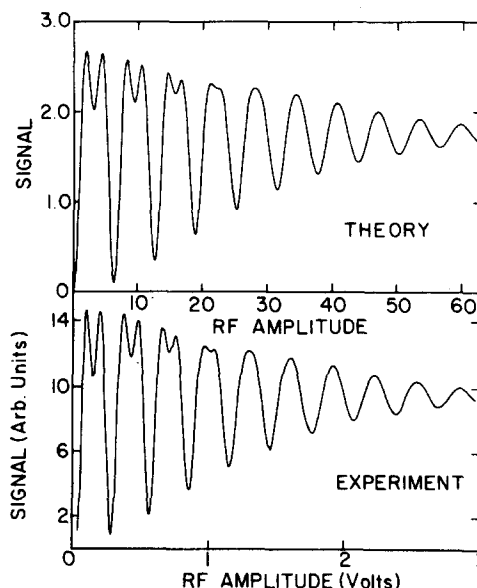
groups. From these results we conclude that the recurrence time, for a constant value of β, is unaffected by the grouping arrangement of the energy levels in the high-field region. On the other hand the oscillatory pattern revealed in the time domain $\beta t = 0, \ldots, 2\pi$ is qualitatively modified by the high-field grouping of the energy levels. While the strong spin–rotation coupling limit results in $2J$ peaks in the amplitude spectra, the asymmetric level grouping according to the correlation diagrams at 7 kG yields a practically smooth single peak, while symmetric splitting leads to the appearance of two pronounced peaks. The latter pattern closely resembles the rf amplitude spectra of the three-level system.

We shall now proceed to confront the results of the model calculations with our experimental data.

VII. EXPERIMENTAL RESULTS

Coherent quantum effects were experimentally studied for three, five, seven, nine, and thirteen-level systems. The experimental results for the oscillatory dependence of the signal on the rf amplitude were quantitatively accounted for in terms of the theory. The theoretical signal functions $S^J(t)$, Eq. (VI. 5), or $\bar{S}^J(t)$, Eq. (VI. 4), were calculated for a single time of flight t through the rf region. In analyzing the experimental data one has to account for the velocity distribution in the supersonic molecular beam, the distribution function being taken in the form[36]

FIG. 11. Experimental data (lower curve) for the dependence of the signal on the intensity of the rf field (on-resonance) for the $(J = 1,\ K = 0)$ Zeeman manifold of O_2^{34} (O^{16}–O^{18}). A mixture of 35% He, 60% Ar, and 5% O_2^{34} (the resonance frequency was 4338 KHz) enriched sample (at total pressure of 750 Torr) was expanded through a 100 μ nozzle. The theoretical curve for the three-level system (upper curve) was calculated from Eq. (VII. 3) with $S^1(t)$ given by Eq. (VI. 6) for $M = 22$.

mental curve in Fig. 11, and all the other experimental curves reported in this work, provide a faithful reproduction of the scans of the xy recorder. The experimental curve for the dependence of the signal on the rf amplitude on-resonance with three-level system is confronted in Fig. 11 with the theoretical prediction for the signal averaged over the velocity distribution given by Eq. (VII.1). The theoretical curve in Fig. 11 was obtained from Eqs. (VII.3) and (VI.6) with $M = 22$. The agreement between theory and experiment is excellent, demonstrating that all the predicted characteristics of the CD of the three-level system exhibiting the oscillatory dependence on the rf amplitude, the maximum signal value of 2.667, the recurrence at $\beta t = 2\pi$, as well as the effects of inhomogeneous dephasing to the asymptotic value of $7/4$, can be experimentally observed.

We have studied experimentally also the rf frequency dependence of the signal at several fixed values of the rf amplitude $\beta t_s = 1.91$, π, 4.37, 2π, and 8.19, which correspond to the first three maxima and to the first two minima in the amplitude spectra of Fig. 11. These spectra for O_2^{34} in the vicinity of the $(J = 1, K = 0)$ transitions are presented in Fig. 12. The linewidth of the central line was found to exhibit a dependence of the form $\beta^{(1/3.5)}$ on the field amplitude, reflecting the effects of power broadening. In Fig. 12 we also portray the theoretical spectra calculated from Eqs. (VI.5a), (V.5), and (V.6), and where the velocity averaging was
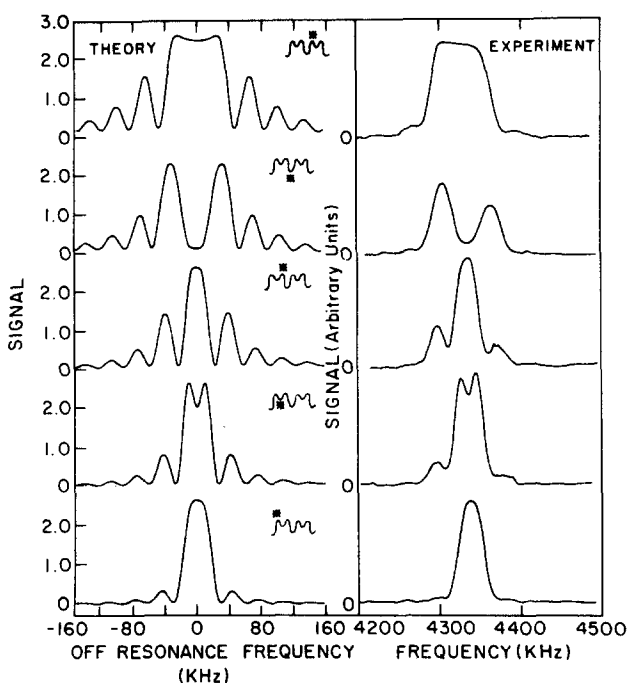

FIG. 13. Experimental results for the rf frequency spectra of the signal for the $(J = 1, K = 1)$ and $(J = 2, K = 1)$ transitions of O_2^{32}. Pure O_2 at 900 Torr was expanded through a 100 μ nozzle. The rf amplitudes are marked in the figure corresponding to the first three maxima and first two minima in the rf amplitude spectra (on-resonance) of the $J = 1$, $K = 1$ three-level system.

FIG. 12. Experimental results of the rf frequency spectra of the signal for the $(J = 1, K = 0)$ transition of $O^{16} - O^{18}$ at several fixed values of the rf amplitude are portrayed in the five curves on the right side. The experimental conditions are as for those of Fig. 11 except that the backing pressure was 450 Torr. The field amplitude was varied to correspond to the first three maxima and two minima of the on-resonance signal of Fig. 11. The five theoretical curves on the left-hand side correspond to the data of Fig. 7 averaged over the velocity distribution according to Eq. (VII.3) with $M = 17$.
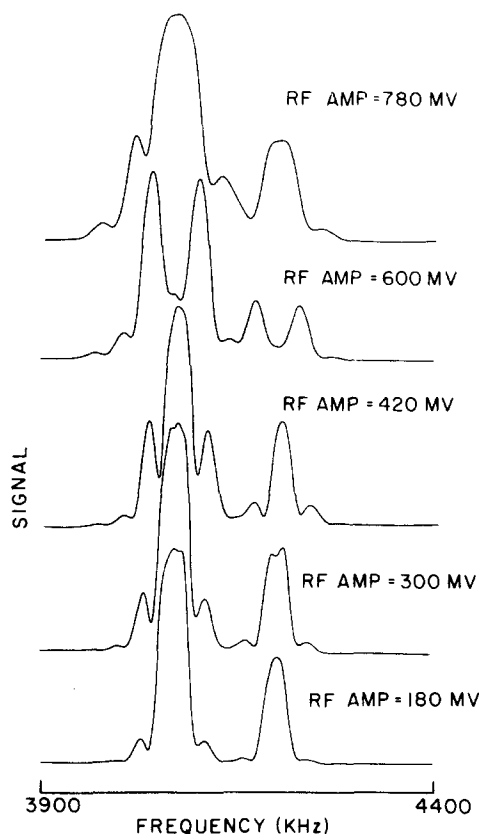
conducted according to Eq. (VI.6). These theoretical spectra display the dependence of the velocity averaged signal on $(\omega - \Omega)$. We note in passing that dephasing effects due to the spread of velocities for high values of $M = 17$ have little effect on the frequency spectra, as is apparent for the comparison of Figs. 11 and 7. The central peaks of the five experimental spectra in Fig. 12 are well reproduced by the theory. At frequencies far above and far below the main peak deviations between theory and experiment are observed as the theory predicts the appearance of symmetric oscillations far off-resonance, while the experimental data reveal a weaker off-resonance modulation, which is asymmetric with respect to positive and negative values of $(\omega - \Omega)$. The discrepancies between theory and experiment is attributed to the oversimplified theoretical treatment of Sec. V, which assumes a sudden switching-on and switching-off of the rf field, while in real life the field is turned on and off adiabatically and quite gradually. The description of the rf field in terms of a step function results in spurious high and low Fourier components in the frequency spectra, which are damped when the field is gradually switched on. This effect is well known for the simple case of a two-level system[37] and similar general features will be exhibited in our multilevel system. Finally, in Fig. 13, we present five experimental frequency spectra taken at the same values
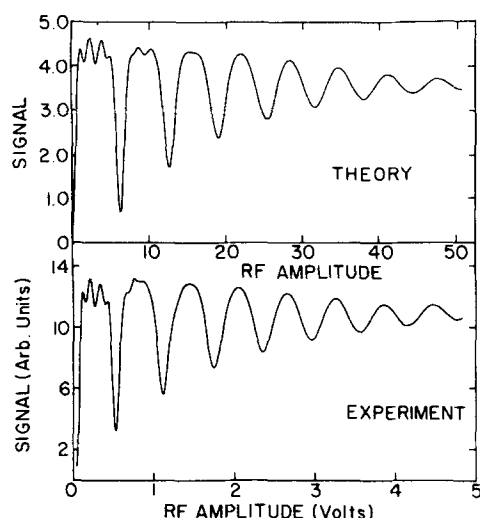
FIG. 14. Experimental results (lower curve) for the dependence of the signal on the intensity of the rf field (on-resonance) for the $(J = 2,\ K = 1)$ manifold of O_2^{32} $(O^{16} - O^{16})$. The resonance frequency was 6455 KHz. A mixture of 80% Ar and 20% O_2^{32} was expanded through a 100 μ nozzle. The backing pressure was 900 Torr. The theoretical data (upper curve) for the five-level system was calculated from Eq. (VII.3) with $S^2(t)$ given by Eq. (VI.7) for $M = 18$.

of βt_s as those in Fig. 12, for the $(J = 1,\ K = 1)$ and for the $(J = 2,\ K = 1)$ states of O_2^{32}. In view of the partial overlap between the two Zeeman manifolds we shall only mention that the features of the $(J = 1,\ K = 1)$ three-level system of O_2^{32} can be qualitatively accounted for in terms of the theoretical curves of Fig. 12.

B. Five-level system

Figure 14 portrays the experimental dependence of the signal on-resonance for the $(J = 2,\ K = 1)$ Zeeman manifold of O_2^{32} on the amplitude of the rf field. The theoretical amplitude spectrum for a five-level system on-resonance (with $M = 18$) also displayed in Fig. 14, is in good overall agreement with the experimental data. At high values of the rf amplitude there is some increase of the experimental signal due to the overlap between the $(J = 2,\ K = 1)$ manifold with the nearby $(J = 1,\ K = 1)$ manifold. The experimental data nicely demonstrate the features of CD of the five-level system, in particular, the maximum amplitude of 4.69, the recurrence at $\beta t = 2\pi$, and the dephasing to the limiting value of 3.6, all of which are observed in real life.

C. Other multilevel systems

We have conducted experimental studies of the rf amplitude spectra on-resonance for several other multilevel systems. Figure 15 presents these experimental results for the $(J = 2,\ K = 2)$, the $(J = 3,\ K = 3)$, the $(J = 4,\ K = 3)$, and the $(J = 6,\ K = 5)$ multilevel systems. Several features of these results should be noted:

(a) The experimental data demonstrate the recurrence of the CD effects in high-dimensional multilevel systems (up to $N = 13$).

(b) Spin–rotation decoupling effects are exhibited for

$K \geqslant 3$ in magnetic field of ~ 7 kG.

(c) The rf amplitude $\beta = 2\pi/t_s$ corresponding to the recurrence of the signal differs for each of the multilevel systems presented in Fig. 15. This is not surprising, as the Rabi frequency (or the transition dipole moment) is different for each of these multilevel systems. From the results of Fig. 15 it is apparent that β increases with increase of the resonance frequency of the Zeeman transition.

(d) The experimental results of Fig. 15 can be qualitatively rationalized in terms of the model calculations of Sec. VI (Figs. 8–10). The $(J = 2,\ K = 3)$ result can be accounted for by Fig. 8(c), the $(J = 3,\ K = 3)$ result corresponds to Fig. 9(b). The $(J = 4,\ K = 3)$ result can be fit by Fig. 10(c). Finally, we note that the $(J = 6,\ K = 5)$ result can be qualitatively accounted for in terms of symmetric grouping of the 13 energy levels into three groups.

(e) The $(J = 3,\ K = 3)$ experimental result provides the only case where the rf amplitude spectrum can be accounted for in terms of the high-field level grouping which corresponds to the correlation diagrams.[26] It should be noted that this is the only multilevel system in Fig. 15 for which level crossing with other M_J states is not exhibited. Only in such case can correlation diagrams be used with confidence. Further work is re-
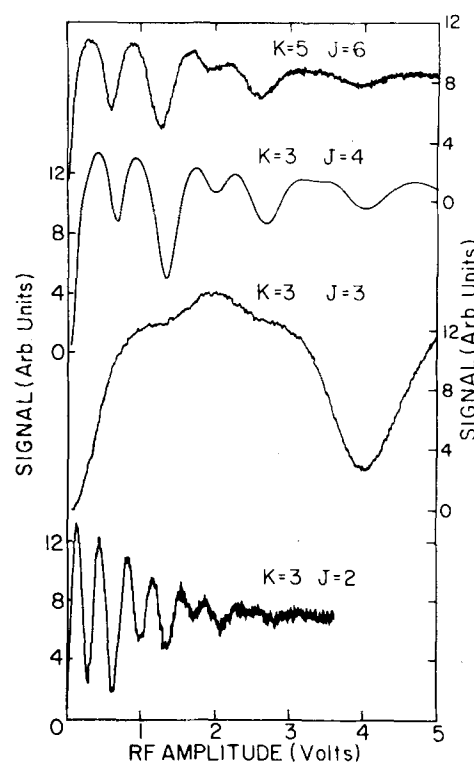

FIG. 15. Experimental rf amplitude spectra on-resonance for different multilevel systems. The spectra for $(K = 3,\ J = 2)$, at the frequency of 2610 KHz, $(K = 3,\ J = 3)$ at the frequency of 795 KHz and $(K = 3,\ J = 4)$ at the frequency of 2289 KHz were obtained by expanding pure O_2 at pressure of 900 Torr through a 100 μ nozzle while the $(K = 5,\ J = 6)$ spectrum at the frequency of 3322 KHz was obtained by expanding O_2 at pressure of 450 Torr through the same nozzle.
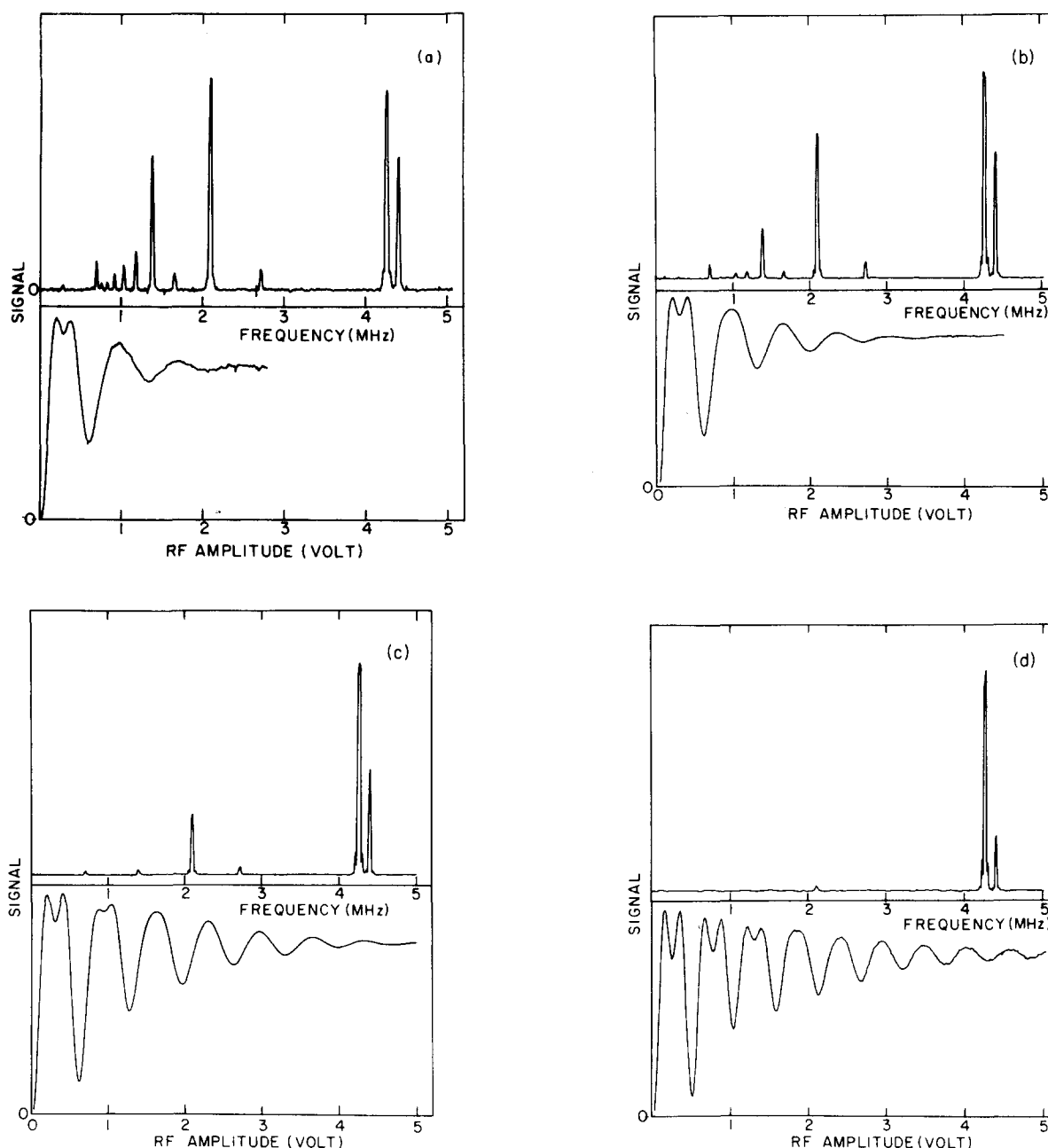
FIG. 16. Experimental rf amplitude spectra on-resonance (lower curves) together with the frequency spectra (upper curves) for O_2^{32}. The nozzle diameter was 100 μ. All the rf amplitude spectra were taken for the $(J=1,\ K=1)$ line. All the rf frequency spectra were obtained for rf amplitude of about 0.17 V, so that the amplitude of the $(J=1,\ K=1)$ line attained its maximum value. (a) O_2 at pressure of 50 Torr; (b) O_2 at pressure of 200 Torr; (c) O_2 at pressure of 900 Torr; (d) 15% O_2 + 85% Ar at pressure of 900 Torr.

quired to elucidate the consequences of level crossing effects.

(f) The experimental ratio of the maxima of the $(J=3, K=3)$ and the $(J=4,\ K=3)$ amplitude spectra is 0.49 ± 0.02. This result is in a very good agreement with the theoretical prediction of 0.505 for this ratio obtained for the level groupings which properly account for the rf dependence of their two amplitude spectra.

VIII. DETERMINATION OF TEMPERATURES IN A SUPERSONIC MOLECULAR BEAM

The inhomogeneous dephasing of the CD effects, manifested by the decrease of the oscillatory amplitude

of the on-resonance signals with increasing of the rf amplitude, provides a novel method for the determination of the velocity distribution in the supersonic beam. Some experimental work in that direction was conducted by Klemperer and colleagues.[22] The dephasing effect of the CD effects can quantitatively be accounted for in terms of a single physical parameter, the Mach number, which can be extracted from the utilization of Eq. (VII.3) and used to evaluate the translational temperature. From the frequency spectra the rotational temperature can be estimated from the relative heights of the lines normalized to their appropriate maximum values, which are predicted by the quantum mechanical calculations and which were experimentally observed.

TABLE II. Temperatures in supersonic molecular beams.

Gas mixture	O_2^{32}	O_2^{32}	O_2^{32}	85% Ar 15% O_2^{32}	65% Ar 30% He 5% O_2 enriched with O^{18}
Nozzle backing pressure (Torr)	50	200	900	900	750
Mach number[a]	4.5 ± 0.5	7.5 ± 0.5	13 ± 0.7	18 ± 1	22 ± 1
T, Translational temperature (°K)[b]	58.6 ± 10	24.2 ± 3.8	8.5 ± 0.8	2.9 ± 0.3	1.8 ± 0.2
T_R, Rotational temperature[c] (°K)	50 ± 5	26.6 ± 2.5	13.0 ± 1.0	5.2 ± 0.4	2.6 ± 0.3
T_{SR}, Spin–rotational temperature[d] (°K)	50 ± 5	25.0 ± 2.5	9.1 ± 1.0	2.8 ± 0.3	3.1 ± 0.3

[a]Mach number is measured from the rf amplitude spectra of $K=1$, $J=1$ three-level systems.
[b]Translational temperature is computed from the Mach number.
[c]Rotational temperature is measured from the $K=3$, $J=4$ and $K=1$, $J=1$ amplitude ratios in O_2^{32} and from the $K=1$, $J=1$ and $K=0$, $J=1$ amplitude ratio in O_2^{34}.
[d]Spin–rotational temperature is measured from the $K=1$, $J=2$ and $K=1$, $J=1$ amplitude ratio.

Thus, the translational, rotational, and spin–rotational temperatures in the supersonic beam can be simultaneously determined.

Figure 16 portrays four rf amplitude spectra of the Zeeman components of the ($J=1$, $K=1$) manifold of O_2^{32} obtained on-resonance, together with the corresponding frequency spectra. The latter frequency spectra were obtained at rf amplitude, where the $J=1$, $K=1$ transition assumes its first maximum value. The four frequency and amplitude spectra were obtained at different stagnation pressures of pure O_2 as well as for an Ar +O_2 mixture. From the rf amplitude spectra the Mach number was evaluated by comparing the experimental curves with the theoretical data for a three-level system on-resonance evaluated from Eqs. (VII. 3) and (VI. 6). These Mach numbers are summarized in Table II, which also includes the results obtained from the analysis of the experimental data of Fig. 11 and Fig. 4. The translational temperature T was extracted from the Mach number by utilizing the relationship[19–21]

$$T = T_0 [1 + (\gamma - 1) M^2/2]^{-1}, \qquad \text{(VIII. 1)}$$

where T_0 is the nozzle stagnation temperature, $\gamma = C_p / C_v$ which is taken as $\gamma = 1.40$ for pure oxygen and $\gamma = 1.62$ for a mixture of 85% Ar plus 15% O_2. The translational temperatures thus obtained are summarized in Table II. The rotational temperature T_R was obtained from the ratio of the amplitudes of two lines, which are characterized by different K values and where rf amplitude spectroscopy was analyzed adequately by us. Appropriate candidates for this analysis are the ($J=1$, $K=1$), ($J=4$, $K=3$), and ($J=3$, $K=3$) transitions.

The rotational temperature T_R was evaluated from the ratio of the maxima $\mathfrak{F}$ of the peaks in the frequency spectrum, which correspond to the ($J=4$, $K=3$) nine-level transitions and to the ($J=1$, $K=1$) three-level transitions. Identical results could be obtained from the amplitude ratio of the ($J=1$, $K=1$) and the ($J=3$,

$K=3$) transitions. The experimental intensity ratio $R_{exp t} = \mathfrak{F}(J=4, K=3)/\mathfrak{F}(J=1, K=1)$ has to be corrected to incorporate the appropriate correction factors for quantum mechanical coherence effects. As we consider the CD of multilevel systems, we cannot get away by just considering the corrections due to the $(2J+1)$ degeneracy factors, as is done for conventional absorption in the presence of external damping. The maxima $\mathfrak{F}$ were obtained for an amplitude of the rf field V, where the ($J=1$, $K=1$) transition assumes its maximum value, so that in our theoretical units $\mathfrak{F}(J=1, K=1) = 2.666$. Two correction factors have to be introduced. First, $\mathfrak{F}(J=4, K=3)$ does not assume its maximum value at the rf amplitude V and from the comparison of the experimental results in Fig. 16(c) for the ($J=1$, $K=1$) system, and in Fig. 15 for the ($J=4$, $K=3$) system, we assert that the latter value of $\mathfrak{F}$ has to be scaled by the numerical factor of 1.288. Second, one has to normalize $R_{exp t}$ by the ratio of the maxima of the signals of the three-level systems, which is 8/3, and for the nine-level system in the spin rotational decoupling mode into three symmetrical groups of levels, which is 7.91, according to Fig. 10(c). The second correction factor is $8/(3 \times 7.91) = 0.337$, which is close to but distinct from the degeneracy ratio. The corrected intensity ratio $R = 1.228 \times 0.337 R_{exp t}$, is fit to the relation $\ln R = \exp[-17.952/T_R]$, where the numerical factor in the exponential is the zero-field splitting[24–27] between the ($J=4$, $K=3$) and the ($J=1$, $K=1$) levels (in K units). The resulting rotational temperatures are presented in Table II.

The spin–rotation temperature T_{SR} was estimated from the ratio of the amplitudes of two lines corresponding to the same K but to different J values. T_{SR} was evaluated from the relative intensities of the ($J=2$, $K=1$) and the ($J=1$, $K=1$) signals in the frequency spectra. The energy gap between these two states is 2.578 °K. Under the experimental conditions utilized

to obtain the spectra of Figs. 16(a)–(c), the spatial separation by the inhomogeneous magnetic field of different M_J components corresponding to the three-level system was adequate, while this separation was somewhat incomplete for the five-level system. Therefore, the spin–rotation temperature was estimated using the following normalization procedure. We have assumed that at the highest temperature studied here $T_R = 50$ K, [corresponding to Fig. 16(a)] $T_{SR} = T_R$. This is a reasonable assumption at $T_{SR} \gg 2.678$ K, where large spin-rotation temperature differences result in small changes of this intensity ratio. This assumption provides us with the necessary normalization factor which enables us to deduce the values of T_{SR} which are summarized in Table II.

The results of Table II provide detailed information on translational, rotational, and spin–rotational temperatures. The velocity distribution in the present magnetic resonance experiment is not affected by the deflecting magnets, so that the measured Mach number provides a lower limit for the actual velocity distribution in the supersonic beam. Our magnetic resonance method for the measurement of the Mach number is superior to the molecular beam electric resonance techniques, where the hexapole electric lens modifies the velocity distribution and increases the apparent Mach number.[38] The Mach numbers obtained by us can be used for a test of the generality of the Anderson–Fenn[36,22] relationship between the terminal Mach number and the product PD, where P(atm) is the stagnation pressure, while D (cm) is the nozzle diameter. Anderson and Fenn have proposed for pure Ar the empirical relation $M = 133 \ (PD)^{0.4}$. We note that our measured value of $M = 22$ in the 60% Ar plus 35% He plus 5% O_2 mixture (with $D = 10^{-2}$ cm) fits this empirical relationship very well for a monoatomic gas. Anderson and Fenn have further proposed[36] the general relationship $M = K (PD)^{(\gamma-1)/\gamma}$. This relationship has not yet been tested for polyatomic gases for which $\gamma \neq 5/3$. Our experimental data for the Mach number for pure O_2 can fit the empirical formula $M = (62.2 \pm 0.1) (PD)^\alpha$ with $\alpha = 0.367 \pm 0.001$. This fit suggests that $\alpha \neq (\gamma-1)/\gamma$ for a diatomic gas and that the Anderson–Fenn empirical relationship does not hold for the general case.

Finally, we would like to comment on some correlations between T, T_R, and T_{SR}. Firstly, we note that at high T and T_R, T_R is close to T, indicating efficient rotational relaxation in the nozzle but that at low temperatures one has $T < T_R$. Secondly, T_{SR} is found to be close to T over the entire temperature range. These results demonstrate how coherent effects in magnetic spectroscopy can be utilized to obtain detailed information on the characteristics of supersonic beams.

IX. CONCLUDING REMARKS

We have adopted the techniques of rf amplitude spectroscopy (RFAS) utilizing a supersonic molecular beam magnetic resonance spectrometer to explore the CD of multilevel systems. It is important to realize that such interrogation of CD can be conducted only in a supersonic beam. From the point of view of general methodo-

logy the spin J system considered herein constitutes one of the few nontrivial exactly soluble (within the RWA, of course) multilevel systems, which can be confronted with experiment. The present work provides quite a detailed confrontation between theory and experiment for a variety of the multilevel systems. The RFAS provides three basic types of information. First, a lot of detailed information emerges regarding the CD of multilevel systems, and how the features of multilevel systems differ from those of the two-level systems. Second, some complementary, useful, but pedestrian data regarding energetics, such as assignment of (JK) levels in low fields and decoupling of rotational and electronic spin at high fields can be obtained. Third, the dephasing of the CD provides a novel way to probe translational and intramolecular temperature in supersonic molecular beams.

APPENDIX A. DYNAMICS OF MULTILEVEL SYSTEMS

We consider the multilevel system described by the Hamiltonian (V.1)–(V.3). Let the initial state at $t = 0$ be $\psi(0) = |JM\rangle$. The time dependent wave function at time t is

$$\psi(t) = \sum_{M'=-J}^{J} C_{MM'}^{J}(t) |JM'\rangle , \qquad (A1)$$

where $C_{MM'}^{J}(t)$ are the transition amplitudes from the initial state $|JM\rangle$ to the state $|JM'\rangle$, which satisfy the equations of motion

$$i\hbar \, \partial C_{MM'}^{J}/dt = E_{JM'} \cdot C_{MM'}^{J} - 2\hbar\beta \sum_{M''=-J}^{J} (J_x)_{M'M''}$$
$$\otimes \, C_{MM''}^{J} \cos(\omega t) . \qquad (A2)$$

Going over to the interaction picture and defining the amplitudes,

$$b_{MM'}^{J}(t) = C_{MM'}^{J}(t) \exp(-iE_{JM'} \cdot t/\hbar) . \qquad (A3)$$

The equations of motion take the form

$$i \partial b_{MM'}^{J}/\partial t = -\beta \sum_{M''=-J}^{J} (J_x)_{M'M''} b_{MM''}^{J}$$
$$\otimes \exp(iD_{M'M''} \cdot t/\hbar)[1 + \exp(\pm 2i\omega t)] . \qquad (A4)$$

where

$$D_{M'M''} = E_{JM'} - E_{JM''} - \hbar\omega \ ; \ E_{JM'} > E_{JM''} , \qquad (A5)$$

$$D_{M'M''} = E_{JM'} - E_{JM''} + \hbar\omega \ ; \ E_{JM'} < E_{JM''} , \qquad (A6)$$

and where $\exp(+2i\omega t)$ appears for the case $E_{JM''} < E_{JM'}$, while $\exp(-2i\omega t)$ stands for the case when $E_{JM''} > E_{JM'}$.

We are now in a position to invoke the rotating wave

approximation (RWA) for the multilevel system, which amounts to neglecting the rapidly oscillatory terms $\exp(\pm 2i\omega t)$ in Eq. (A4). The conditions for the applicability of the RWA for a multilevel system are somewhat more subtle than for the common case of a two-level system. Sufficient conditions for the RWA to apply for a N level system are,[7] (a) smallness of radiative coupling $\beta \ll \omega$ which is reasonably well satisfied, and (b) smallness of off-resonance energies, Eqs. (A5) and (A6), i.e., $|D_{MM'}| \ll \hbar\omega$ for all M and M'. This condition holds as radiative coupling is governed by the selection rule $\Delta M = \pm 1$. The RWA equations of motion for the equally spaced level system, where radiative coupling prevails between adjacent states is

$$i\partial b^J_{MM'}/\partial t = -\beta \sum_{M''=-J}^{J} (J_x)_{M'M''} b^J_{MM''}$$
$$\otimes \exp(iD_{M'M''}t/\hbar) . \tag{A7}$$

Finally, one can transform to a rotating frame by defining a third kind of transition amplitudes

$$a^J_{MM'}(t) = C^J_{MM'}(t) \exp(-i\overline{E}_{JM'}t) , \tag{A8}$$

with

$$\overline{E}_{JM'} = E_{JM'} + (J - M')\hbar\omega \tag{A9}$$

being the energies of "dressed" molecule–photon states, we get

$$i\partial a^J_{MM'}/\partial t = (\overline{E}_{JM'}/\hbar) a^J_{MM'} - \beta \sum_{M''=-J}^{J} (J_x)_{M'M''} a^J_{MM''} . \tag{A10}$$

APPENDIX B. THE SPIN J PROBLEM

The Hamiltonian for a single (JK) linear Zeeman manifold is

$$H = -\hbar\Omega[J_z + 2\lambda J_x \cos(\omega t)] , \tag{B1}$$

with $-\Omega = f(K_J)$ and $\lambda = \beta/\Omega$. Following Gottfried,[32] we define unit vectors $\hat{\mu}_c(t)$ and $\hat{\mu}_a(t)$, which rotate about the unit vector $\hat{\mu}_z$ (in the z direction) with frequency ω in the clockwise and in the anticlockwise directions, respectively,

$$\hat{\mu}_c(t) = \hat{\mu}_x \cos(\omega t) - \hat{\mu}_y \sin(\omega t) ,$$
$$\hat{\mu}_a(t) = \hat{\mu}_x \cos(\omega t) + \hat{\mu}_y \sin(\omega t) , \tag{B2}$$

so that

$$H = -\hbar\Omega[J_z + \lambda(J \cdot \hat{\mu}_c(t) + J \cdot \hat{\mu}_a(t))] . \tag{B3}$$

Invoking the RWA one can drop the anticlockwise term, and noting that

$$J \cdot \hat{\mu}_c(t) = \exp(i\omega t J_z) J_x \exp(-i\omega t J_z) \tag{B4}$$

the RWA Schrödinger equation is

$$i\partial\psi(t)/\partial t = -\Omega[J_z + \lambda \exp(i\omega t)J_x$$
$$\otimes \exp(-i\omega t J_z)]\psi(t) . \tag{B5}$$

Now letting

$$|\tau\rangle = \exp(-i\omega t J_z)\psi(t) , \tag{B6}$$

one gets

$$i\frac{\partial}{\partial t}|\tau\rangle = [(\omega - \Omega)J_z - \lambda\Omega J_x]|\tau\rangle , \tag{B7}$$

whose solution is

$$= \exp[-i\Delta\hat{J} \cdot \hat{n}t]|0\rangle , \tag{B8}$$

where

$$\Delta^2 = (\omega - \Omega)^2 + \beta^2 \tag{B9}$$

and

$$\hat{n} = \hat{\mu}_z \cos\phi + \hat{\mu}_x \sin\phi , \tag{B10}$$

with

$$\tan\phi = -\beta/(\omega - \Omega) . \tag{B11}$$

Equation (B6) now reads

$$\psi(t) = \exp(i\omega t J_z) \exp(-i\Delta\hat{J} \cdot \hat{n}t)\psi(0) . \tag{B12}$$

Let $\psi(0) = |JM\rangle$, then the probability amplitude for finding the system in the state $|JM'\rangle$ at the time t is

$$C^J_{MM'}(t) = \exp(iM'\omega t)\langle JM'|\exp(-i\Delta\hat{J} \cdot \hat{n}t)|JM\rangle . \tag{B13}$$

The probability $P^J_{MM'}(t)$, Eq. (14), is then

$$P^J_{MM'}(t) = |\langle JM'|\exp(-i\Delta\hat{J} \cdot \hat{M}t)|JM\rangle|^2 , \tag{B14}$$

which leads to Eq. (V.4).

APPENDIX C. THE $d^J_{MM'}(\alpha)$ FUNCTIONS

We list here the d functions which are useful for the analysis of the coherent dynamics of $N = 3$, 5, and 7 systems for both on-resonance and for off-resonance coupling. Numerical calculations were performed using Eq. (V.6) up to $N = 13$. The missing d functions are easily obtained from those given here by using the symmetry relations

$$d^J_{MM'}(\alpha) = (-1)^{M-M'} d_{-M-M'}(\alpha) ,$$
$$d^J_{M'M}(\alpha) = (-1)^{M-M'} d_{MM'}(\alpha) .$$

The explicit expressions are

$$J = 1 ; \quad \begin{array}{ll} d_{11}(\alpha) = \frac{1}{2}(1 + \cos\alpha) , & d_{01}(\alpha) = (\sin\alpha)/\sqrt{2} \\ d_{1-1}(\alpha) = \frac{1}{2}(1 - \cos\alpha) , & d_{00}(\alpha) = \cos\alpha . \end{array}$$

$$\begin{array}{ll} d_{22}(\alpha) = \frac{1}{4}(1 + \cos\alpha)^2 , & d_{21}(\alpha) = -\frac{1}{2}(1 + \cos\alpha)\sin\alpha , \\ d_{20}(\alpha) = (\sqrt{6}/4)\sin^2\alpha , & d_{2-1}(\alpha) = -\frac{1}{2}(1 - \cos\alpha)\sin\alpha , \end{array}$$
$$J = 2 ; \quad \begin{array}{ll} d_{2-2}(\alpha) = \frac{1}{4}(1 - \cos\alpha)^2 , & d_{11}(\alpha) = \frac{1}{2}(1 + \cos\alpha)(2\cos\alpha - 1) , \\ d_{10}(\alpha) = -(\frac{3}{2})^{1/2}\sin\alpha\cos\alpha , & d_{1-1}(\alpha) = \frac{1}{2}(1 - \cos\alpha)(2\cos\alpha + 1) , \end{array}$$
$$d_{00}(\alpha) = \frac{1}{2}(3\cos^2\alpha - 1)$$

$$d_{33}(\alpha) = \tfrac{1}{8}(1 + \cos\alpha)^3 ,$$

$$d_{31}(\alpha) = (15^{1/2}/8)\sin^2\alpha(1 + \cos\alpha) ,$$

$$d_{3\text{-}1}(\alpha) = (15^{1/2}/8)\sin^2\alpha(1 - \cos\alpha) ,$$

$$J = 3 \; ; \qquad d_{3\text{-}3}(\alpha) = \tfrac{1}{8}(1 - \cos\alpha)^3 ,$$

$$d_{21}(\alpha) = -(5^{1/2}/4\sqrt{2})\sin\alpha(3\cos^2\alpha + 2\cos\alpha - 1) ,$$

$$d_{2\text{-}1}(\alpha) = (5^{1/2}/4\sqrt{2})\sin\alpha(3\cos^2\alpha - 2\cos\alpha - 1) ,$$

$$d_{11}(\alpha) = \tfrac{1}{8}(1 + \cos\alpha)(15\cos^2\alpha - 10\cos\alpha - 1) ,$$

$$d_{1\text{-}1}(\alpha) = \tfrac{1}{8}(1 - \cos\alpha)(15\cos^2\alpha + 10\cos\alpha - 1) ,$$

$$d_{32}(\alpha) = -(6^{1/2}/8)\sin\alpha(1 + \cos\alpha)^2 ,$$

$$d_{30}(\alpha) = -(5^{1/2}/4)\sin^3\alpha ,$$

$$d_{3\text{-}2}(\alpha) = -(6^{1/2}/8)\sin\alpha(1 - \cos\alpha)^2 ,$$

$$d_{22}(\alpha) = \tfrac{1}{4}(1 + \cos\alpha)^2(3\cos\alpha - 2) ,$$

$$d_{20}(\alpha) = (15^{1/2}/2\sqrt{2})\cos\alpha\sin^2\alpha ,$$

$$d_{2\text{-}2}(\alpha) = \tfrac{1}{4}(1 - \cos\alpha)^2(3\cos\alpha + 2) ,$$

$$d_{10}(\alpha) = -(\sqrt{3}/4)\sin\alpha(5\cos^2\alpha - 1) ,$$

$$d_{00}(\alpha) = (5\cos^3\alpha - 3\cos\alpha)/2 .$$

APPENDIX D. DYNAMICS OF EQUALLY SPACED, EQUALLY COUPLED SYSTEMS

We consider first the general discrete level system characterized by the Hamiltonian

$$H = -\hbar\Omega J_z + \hbar\gamma \mathbf{A}\cos(\omega t) , \tag{D1}$$

where γ is a coupling strength and matrix $\mathbf{A}$ is triagonal.

Denoting the N eigenvalues of $-\hbar\Omega J_z$ as $(I = 1, 2, \ldots, N)$ with energies E_I the RWA equations of motion, which are equivalent to Eq. (A.11) are

$$i\partial a_{I'}/\partial t = \overline{E}_{I'} a_{I'}/\hbar + \gamma[A_{I',I'+1}a_{I'+1} + A_{I',I'-1}a_{I'-1}] \tag{D2}$$

with

$$\overline{E}_{I'} = E_{I'} + (N - I')\hbar\omega , \tag{D2a}$$

which can be written in the concise form

$$i\hbar\partial \mathbf{a}/\partial t = \mathbf{H}\mathbf{a} , \tag{D3}$$

where $a(t)$ is the vector of the amplitudes $a_I(t)$, the initial conditions being characterized by $a(0)$, and $\mathbf{H}$ is the Hamiltonian matrix for the "dressed" states. The Hamiltonian matrix can be diagonalized by the unitary transformation $\mathbf{V}$, so that $\mathbf{V}^{-1}\mathbf{H}\mathbf{V} = \Lambda$ where Λ is the diagonal matrix of the N eigenvalues λ_1, λ_2–λ_N. The time dependent amplitudes are

$$\mathbf{a}(t) = \mathbf{V}\exp(-i\Lambda t)\mathbf{V}^{-1}\mathbf{a}(0) . \tag{D4}$$

The matrix elements of V will be denoted as $V_M(\lambda_K)$, being labeled in terms of the corresponding eigenvalues.

The probability $P_{MM'}(t)$ that the system be found in state $|M'\rangle$ at time t if it was initially (at $t = 0$) in the state $|M\rangle$ can be expressed explicitly as

$$P_{MM'}(t) = \sum_K \sum_L \exp[i(\lambda_K - \lambda_L)t]$$

$$\otimes V_{M'}(\lambda_K)V_M^*(\lambda_K)V_{M'}^*(\lambda_L)V_M(\lambda_L) .$$

Consider now the special case of the ESEC system where the matrix $\mathbf{A}$ is

$$\mathbf{A} = \begin{pmatrix} 0 & 1 & 0 & \cdots \\ 1 & 0 & 1 & \cdots \\ 0 & 1 & 0 & \cdots \end{pmatrix} \tag{D6}$$

and let us specialize to the case of resonance coupling so that all the diagonal energies in the Hamiltonian matrix are zero. The dynamics of this radiatively driven model system now reduces to the well-known Huckel problem or the classical mechanics of N harmonically coupled harmonic oscillators. The eigenvalues are

$$\lambda_K/\gamma = \cos(K\pi/(N+1)) ; \quad K = 1, 2, \ldots, N , \tag{D7}$$

while the eigenvectors are given by

$$V_M(\lambda_K) = [2/(N+1)]^{1/2}\sin(MK\pi/(N+1)) \tag{D8}$$

It can easily be shown by simple algebraic manipulations that for the special case of $N = 3$ ESEC systems the results obtained from Eqs. (D5), (D7), and (D8) are identical with those derived by using Eq. (V.4) for $J = 1$ in the on-resonance situation, provided that we set $\beta - V\sqrt{2}/2$.

[1](a) L. Allen and J. H. Eberly, *Optical Resonance and Two-Level Atoms* (Wiley, New York, 1975); (b) M. Sargent III, M. O. Scully, and W. E. Lamb, Jr., *Laser Physics* (Addison Wesley, Reading, Mass., 1974).

[2](a) D. Grischkowsky, M. M. T. Lory, and P. F. Liao, Phys. Rev. A 12, 2514 (1975); (b) R. G. Brewer and E. L. Hahn, Phys. Rev. A 11, 1641 (1975); (c) D. G. Gold and E. L. Hahn, Phys. Rev. A 16, 324 (1977); (d) H. Hatanaka and T. Hashi, J. Phys. Soc. Jpn. 39, 1139 (1975); (e) M. Sargent III and P. Horwitz, Phys. Rev. A 13, 1962 (1976); (f) A. Schenzle and R. G. Brewer, Phys. Rep. 43, 455 (1978).

[3](a) N. Bloembergen, Opt. Comm. 15, 416 (1975); (b) D. M. Larsen and N. Bloembergen, Opt. Commun. 17, 254 (1976).

[4] V. S. Letokhov and A. A. Makarow, Opt. Commun. 17, 250 (1976).

[5] S. Mukamel and J. Jortner, Chem. Phys. Lett. 40, 159 (1976); J. Chem. Phys. 65, 5204 (1976).

[6](a) J. H. Eberly, B. W. Shore, Z. Bialynicka-Birula, and I. Bilynicki-Birula, Phys. Rev. 16, 2038 (1977); (b) Z. Bialynicka-Birula, I. Bilynicki-Birula, J. H. Eberly, and B. W. Shore, Phys. Rev. A 16, 2048 (1977).

[7] I. Shek and J. Jortner, Chem. Phys. Lett. 63, 5 (1979).

[8](a) D. Cantrell and K. Fox, Opt. Lett. 2, 151 (1978); (b) J. R. Ackerhalt and H. W. Galbraith, J. Chem. Phys. 69, 179 (1976).

[9] R. R. Freeman, E. M. Mattison, D. E. Pritchard, and D. Kleppner, J. Chem. Phys. 64, 1194 (1976).

[10] E. M. Mattison, D. E. Pritchard, and D. Kleppner, Phys. Rev. Lett. 32, 507 (1974).

[11] N. R. Isenor and M. R. Richardson, Appl. Phys. Lett. 18, 225 (1971).

[12] N. Bloembergen and E. Yablonovitch, Phys. Today 31, 23 (1978).

[13] C. D. Cantrell, S. M. Freund, and J. L. Lyman, in *Laser Handbook* (North-Holland, Amsterdam, 1978), Vol. III(b).

[14] A. Yogev, Paper presented at Laser Chemistry Conference, Ein Bokek, December, 1978.

[15]S. A. Tuccio, J. H. Dubrin, O. G. Peterson, and B. B. Snavely, IEEE Quantum Electron. 10, 790 (1974).

[16]A. Amirav and U. Even, "Isotope separation from supersonic molecular beam," J. Appl. Phys. 51, 1 (1980).

[17]N. F. Ramsey, Molecular Beams (Oxford University, London, 1956).

[18]P. Kusch and V. W. Hughes, Handbuch der Physik (Springer, Berlin, 1959), Vol. 37/1, p. 1.

[19]T. A. Milne and F. T. Greene, Adv. High Temp. Chem. 2, 107 (1969).

[20]J. B. Anderson, R. P. Andress, and J. B. Fenn, Adv. Chem. Phys. 10, 275 (1965).

[21]H. Pauly and J. P. Toennies, Methods of Experimental Physics, edited by B. Bedersand and W. Fife (Academic, New York, 1968), Vol. 7A, p. 227.

[22]T. R. Dyke, G. R. Tomasevich, and W. Klemperer, J. Chem. Phys. 57, 2277 (1972).

[23]L. S. Goodman, Rev. Sci. Instr. 31, 1351 (1960).

[24]A. F. Henry, Phys. Rev. 80, 396 (1950).

[25]M. Tinkham and M. W. P. Strandberg, Phys. Rev. 97, 937 (1955).

[26]M. Tinkham and M. W. P. Strandberg, Phys. Rev. 97, 951 (1955).

[27]J. M. Hendrie and P. Kusch, Phys. Rev. 107, 716 (1957).

[28]E. Majorana, Nuovo Cimento 9, 43 (1932).

[29]F. Bloch and I. I. Rabi, Rev. Mod. Phys. 17, 237 (1945).

[30]J. Schwinger, On Angular Momentum Nuclear Development Associates (1952).

[31]Reference (17) Appendix E.

[32]K. Gottfried, Quantum Mechanics (Benjamin, New York, 1966), Vol. 1, Sec. 55.

[33]A. Messiah, Quantum Mechanics (Wiley, New York, 1961).

[34]A. A. Maradudin, E. W. Montroll, and G. W. Weiss, Theory of Lattice Dynamics in the Harmonic Approximation (Academic, New York, 1963).

[35]See for example, R. Dandel, R. Lefebvre, and C. Moser, Quantum Chemistry (Interscience, New York, 1959).

[36]J. B. Anderson and J. B. Fenn, Phys. Fluids 8, 780 (1965).

[37]J. H. Shirley, Phys. Rev. 160, 95 (1967).

[38]B. G. Wicke, J. Chem. Phys. 63, 1035 (1975).